Available online at www.sciencedirect.com
ScienceDirect
Journal of Nuclear Materials 371 (2007) 314–328
journal of nuclear materials
www.elsevier.com/locate/jnucmat

Irradiation tests of mixed-oxide fuel prepared with weapons-derived plutonium

L.J. Ott [a,*], R.N. Morris [b,1]

[a] Nuclear Science and Technology Division, Oak Ridge National Laboratory, P.O. Box 2008, MS 6167, Oak Ridge, TN 37831, United States
[b] Materials Science and Technology Division, Oak Ridge National Laboratory, P.O. Box 2008, MS 6167, Oak Ridge, TN 37831, United States

Abstract

Mixed-oxide test capsules prepared with weapons-derived plutonium have been irradiated to a burnup of 50 GWd/MT. The mixed-oxide fuel was fabricated at Los Alamos National Laboratory by a master-mix process and has been irradiated in the advanced test reactor at the Idaho National Laboratory. Previous withdrawals of the same fuel have occurred at 9, 21, 30, and 40 GWd/MT. Oak Ridge National Laboratory manages this test series for the Department of Energy's Fissile Materials Disposition Program. This paper describes the preparation of the mixed-oxide fuel, the equipment design, and the irradiation history of the test capsules, and discusses the significance of the more important observations of the post-irradiation examinations. Code predictions (FRAPCON-3 and TRANSURANUS) are presented and compared with available post-irradiation examination data for the highest and lowest powered mixed-oxide capsules. Fuel performance has been excellent and consistent with code predictions and with existing US and European experience.
Published by Elsevier B.V.

1. Introduction

The United States Department of Energy Fissile Materials Disposition Program (FMDP) is pursuing disposal of surplus weapons-usable plutonium by reactor irradiation as the fissile constituent of MOX fuel [1]. A large body of MOX fuel irradiation experience exists through the genesis of research, development, and deployment programs primarily in Europe over the last four decades. Most of this experience has been gained with reactor-grade plutonium, as derived from spent low-enriched uranium fuel. Since 1998, a test irradiation [2] of mixed-oxide (MOX) fuel prepared with weapons-derived plutonium has been conducted at the Idaho National Laboratory (INL) in the advanced test reactor (ATR).

Weapons-derived MOX fuel differs from the commercial fuel utilized in Europe in that its initial fissile inventory comprises a higher proportion of ^{239}Pu, with smaller contingents of the higher plutonium isotopes, and because the plutonium may be accompanied by small amounts of gallium as an impurity. The present test irradiation supports the

* Corresponding author. Tel.: +1 865 574 0324; fax: +1 865 574 2032.
E-mail addresses: ottlj@ornl.gov (L.J. Ott), morrisrn@ornl.gov (R.N. Morris).
[1] Tel.: +1 865 241 4237; fax: +1 865 576 7862.

0022-3115/$ - see front matter Published by Elsevier B.V.
doi:10.1016/j.jnucmat.2007.05.030

disposition mission by demonstrating that introduction of weapons-derived plutonium does not compromise the applicability of the existing MOX database. Oak Ridge National Laboratory manages this irradiation demonstration project for the Department of Energy.

2. Test capsule and fuel pin design

Fig. 1 illustrates the fuel pin and capsule cross-section. The pellet size and Zircaloy-4 cladding thickness are typical of commercial PWR fuel. The initial gap between pellet and cladding is narrower, however – about 50 μm as opposed to 150–200 μm diametral in typical PWR fuel. The gap between cladding and capsule is also small. The absence of water at the outer surface of the cladding precludes hybriding so that loss of cladding ductility is limited to that caused by irradiation hardening or any effects of fuel impurities such as gallium.

Fig. 2 is an elevation view of one of the simple uninstrumented drop-in capsule assemblies. There are 15 MOX pellets in each 152 mm fuel pin pellet stack. The fill gas for the fuel pins and capsules is helium at atmospheric pressure. A gas collection plenum is provided at the top of each fuel pin (surrounding the stainless steel spring).

3. Test assembly

The test capsules were secured within a test assembly and irradiated initially in the small North-

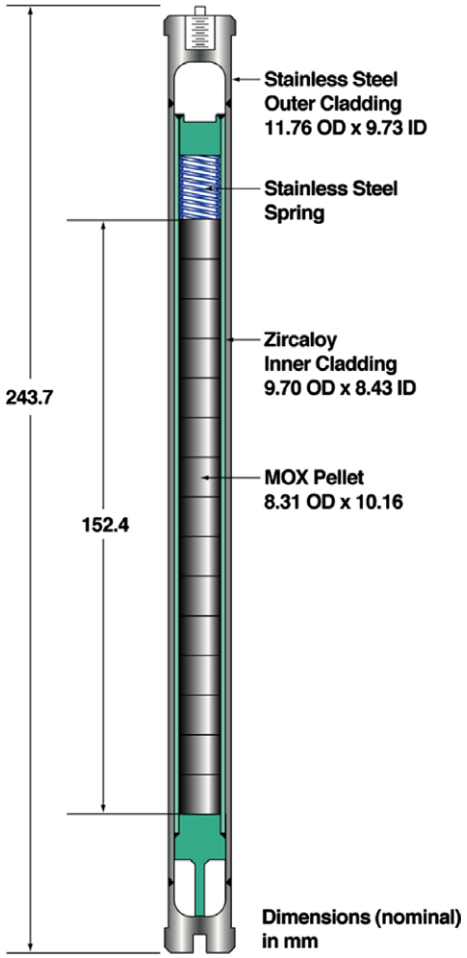

Fig. 2. Each capsule assembly contains one Zircaloy fuel pin with 15 fuel pellets.

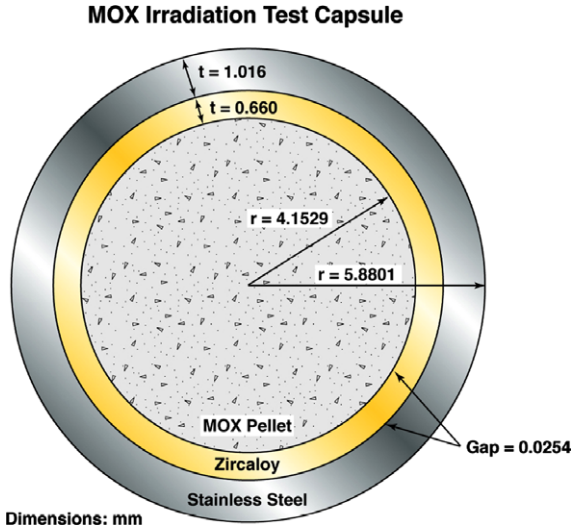

Fig. 1. A stainless steel capsule contains each fuel pin.

west I-hole of the ATR reflector. The test assembly provided nine capsule positions, as shown in Fig. 3. As the fueled capsules were withdrawn for PIE, solid stainless steel capsule simulators filled any test assembly positions not occupied by MOX test capsules.

As shown in the basket assembly cross-section at the top of Fig. 3, the capsule columns are arranged with two in front (in the direction of the ATR core) and one behind. The test assembly is aligned vertically such that the midplanes of the middle capsules correspond to the midplane of the ATR core. Thus, the highest thermal fluxes (and axial powers) are found for the capsules at the two front middle positions with descending fluxes for the capsules placed at the front top and bottom, back middle, and back top and bottom positions. As an example, for the initial heatup

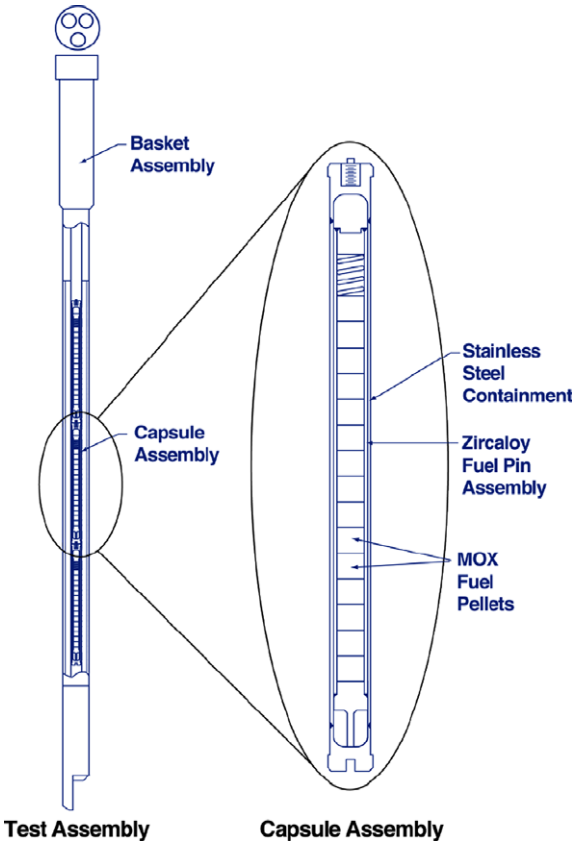

Fig. 3. The test assembly permitted simultaneous irradiation of up to nine MOX test capsules.

with all nine positions occupied by fresh fuel, the linear heat generation rates (LHGRs) ranged from 30.2 kW/m at the front middle to 20.3 kW/m in the back top and bottom positions.

The thermal and fast flux profiles along the three capsule positions in each column were determined at intervals of approximately 100 effective full-power days (EFPDs) throughout the irradiation by means of flux wires. It was desirable during the course of the irradiation to maintain high LHGRs by increasing the thermal flux at the fuel to counter the effects of plutonium depletion. This was accomplished first by shifting from an Inconel-shielded basket assembly to a basket assembly with an aluminum shield after the first 155 EFPDs. Later, at about 800 EFPDs, the test assembly was shifted to the higher-flux Southwest I-hole position within the ATR reflector.

Because the upper and lower ends of the pellet stack are unshielded, the end pellets receive more thermal flux and hence there is end peaking in the fuel stack.

4. Preparation of the MOX test fuel

The MOX fuel for this test irradiation was fabricated during 1997 at the Los Alamos National Laboratory via a master-mix process. This mixed-oxide comprises 5% PuO_2 and 95% depleted UO_2, the latter converted by the ammonium diuranate (ADU) process. All of the PuO_2 was introduced as 31% of the master-mix.

The secondary blending (dilution) process by which the master-mix was distributed into the depleted UO_2 matrix was incomplete, in the sense that residual particles (agglomerates) of the master-mix remain intact within the final blend. The equivalent diameters for the test fuel agglomerates range from very small to quite large, with about 1.5% of the fuel cross-section area occupied by particles with equivalent diameters of 400 μm or more.

The mission fuel will be improved relative to the weapons-derived mixed-oxide fuel discussed in this paper. Lead test assembly (LTA) and mission fuel will have a lower plutonium concentration (4.4% compared to test concentrations of 5%) with a maximum PuO_2 of 20% in the master mix. Also, use of modern fuel fabrication techniques will increase the PuO_2 homogenization within the fuel and reduce agglomerate size (with a maximum agglomerate size of 100 μm). It is expected that these improvements will result in lower fission gas releases.

Weapons-derived plutonium includes the alloying agent gallium at approximately 1 wt%. Of the 11 capsules irradiated, five were loaded with pellets prepared from PuO_2 powder that had been thermally treated for gallium removal [3]. Whether or not the small quantity of gallium carried into the finished MOX fuel has the potential to adversely affect fuel and cladding performance was among the technical issues addressed by this test.

5. Irradiation histories [4]

Irradiation began in February 1998 and continued through to April 2004 for a total of 11 MOX test capsules. The predicted operating envelope (linear heat generation rates (LHGRs), fuel temperatures) for the MOX test irradiation is prototypic of commercial light water reactors (LWRs) with fuel of similar dimensions.

The ATR irradiation cycles have been grouped into ‘phases’, as indicated in Table 1. In general, each irradiation phase defines a different arrangement of capsules (and capsule simulators) within

Table 1
The paired MOX test capsules (normal and TIGR[a]-treated) have been withdrawn sequentially

Irradiation phase	Date completed	Effective full power days	Capsules withdrawn	Burnup (GWd/MT)
I	September 13, 1998	154.9	1 and 8	8.8
II	September 12, 1999	227.7	2 and 9	21.0
III (Part 1)	July 23, 2000	232.4	3 and 10	30.2
III (Part 2[b])	January 14, 2001	113.1	–	–
IV (Part 1)	March 9, 2002	289.1	4 and 13	39.8
IV (Parts 2 and 3)	April 18, 2004	444.6	5, 6, and 12	50.0

[a] TIGR = thermally-induced gallium removal [3].
[b] Phase III (Part 2) provided catch-up irradiation for Capsules 5, 6, and 12 only.

Table 2
Average as-run LHGRs (kW/m) for 9-, 21-, 30-, and 40-GWd/MT withdrawn capsules

Irradiation phase	EFPDs	Burnup	9 GWd/MT		21 GWd/MT		30 GWd/MT		40 GWd/MT	
		Capsule	1	8	2	9	3	10	4	13
I	154.9		27.0	27.1	26.0	26.5	25.8	26.5	19.2	19.4
II	227.7				26.9	27.1	26.5	27.2	29.5	29.9
III – Part 1	232.4						17.7	18.3	18.6	18.8
IV – Part 1	289.1								17.0	17.1
		FGR (%)			1.32	1.88	1.47	2.30	8.37	9.51

the test assembly. Table 1 also provides the MOX capsule withdrawal schedule and the associated burnups.

The average as-run LHGRs are listed in Table 2 for the test MOX capsules withdrawn at burnups of 9-, 21-, 30-, and 40-GWd/MT and in Table 3 for the 50 GWd/MT test MOX capsules.

In general, the average LHGR operating range for commercial PWRs is 16.4–23 kW/m. The expected average LHGR for the MOX mission fuel is approximately 18.4 kW/m (21 kW/m for the LTAs at BOL). Ten of the MOX test capsules operated at conservatively higher LHGRs than the expected mission conditions; thus, the test fuel experienced higher fuel temperatures than is expected for the mission fuel.

Table 3
Average as-run LHGRs (kW/m) for 50-GWd/MT Capsules

Irradiation phase	EFPDs	Capsule		
		5	6	12
I	154.9	20.0	–	–
II	227.7	23.1	25.0	25.3
III – Part 1	232.4	17.9	19.0	19.2
III – Part 2	113.1	13.3	20.8	21.2
IV – Part 1	289.1	13.6	17.8	17.9
IV – Part 2	110.2	16.6	19.0	19.3
IV – Part 3	334.4	12.6	13.7	14.0
	FGR (%)	3.37	7.22	8.61

6. PIE schedule

As indicated in Table 1, ten capsules have been withdrawn for post-irradiation examination (PIE) in sequential sets of symmetrically-loaded pairs (TIGR–non-TIGR), at burnups of 9-, 21-, 30-, 40-, and 50-GWd/MT. The 11th capsule (non-TIGR Capsule 5) was also withdrawn at 50 GWd/MT.

The PIEs [5] included visual and dimensional inspection, gamma scanning, metallography, fuel and cladding gallium analyses, fission gas release determination, and burnup analyses. Of particular interest were any fuel-cladding interaction effects. Residual cladding strength is determined by post-irradiation testing. The stainless steel capsule protects the outer surface of the cladding, so there is no embrittlement by clad hydriding (as normally induced in commercial reactors) to mask any detrimental effects that might be introduced by the special nature of this fuel.

To date, PIE has been completed for the 11 capsules withdrawn with burnups of 9-, 21-, 30-, 40-, and 50-GWd/MT. Fuel performance including cladding integrity has been excellent.

7. Overview of significant PIE observations

This mixed-oxide test irradiation was carried out under conditions more severe than will be

encountered by the mission fuel in the US commercial reactors participating in the Fissile Materials Disposition Program. Individual capsule linear heat generation rates and fuel temperatures depend upon the location of the capsule within the test assembly during irradiation but in general were higher than those expected for mission fuel. All of the post-irradiation examinations have been conducted at the Irradiated Fuels Examination and Radioactive Materials Analysis Laboratories at Oak Ridge National Laboratory. The following discussions provide an overview of the more significant PIE observations.

7.1. Agglomerates and fission gas release

For the MOX fuel prepared for this test irradiation, all of the PuO_2 was introduced as 31% of the master-mix. After dilution into the remainder of the UO_2, the equivalent diameters of the residual master-mix particles (agglomerates) in the final blend ranged from very small to 400 μm or more. The presence of a few large agglomerates confirms that the secondary blending (dilution) process was incomplete in this test fuel, but is beneficial from the standpoint of insights as to the effects of agglomerate size to be gleaned from the post-irradiation analyses.

Sections of fuel and surrounding cladding have been examined by both scanning electron microscope (SEM) and electron probe microanalysis (EPMA). Areas of particular interest include the nature of the large agglomerates and their immediate surroundings.

High burnup within the plutonium-rich agglomerates is accompanied by considerable local swelling induced by the accumulated solid and gaseous fission products. Whereas the solid fission products stay with an agglomerate throughout fuel life, the fate of the fission product gases depends upon the temperature during irradiation of the region in which the agglomerate is located. (Even the largest of the agglomerates are still sufficiently small that their internal temperatures only slightly exceed that of the immediately surrounding UO_2 matrix.)

Agglomerates become highly visible when they have transformed into a 'high burnup structure'. In general, a high burnup structure (small grains with a few large pores) evolves during irradiation when the local temperature is less than 1000 °C and the local burnup exceeds about 60 GWd/MT. Prior to transformation, much of the fission gas is stored in nanometer-size cavities within the approximately 10-μm fuel grains. Subsequent to transformation, the grains are in the 0.5- to 1.0-μm range, in a structure interspersed with relatively large gas storage pores. Much of the gas displaced from the very small intergranular cavities is collected (at high pressure) in the facetted pores in the recrystallized microstructure.

Agglomerates in the outer region of the MOX test fuel mounts are clearly visible due to their high-burnup structure. See Fig. 4 for a fuel cross section micrograph at 40 GWd/MT. The halos around these agglomerates are fission products in the surrounding UO_2 grains, which either diffused (primarily athermally) prior to transformation or were displaced when the high burnup structure was formed. The large size of the agglomerates and the aggressive irradiation conditions of the 40 GWd/MT fuel pins were favorable to the development of three regions with different polishing characteristics (which made the structure visible): the agglomerate with its small grains, the halo composed of nearby matrix with local damage from recoils, and the relatively undamaged distant matrix. Faint agglomerate outlines can be discerned in the central regions of these fuel mounts at a fuel-average burnup of 40 GWd/MT. These are

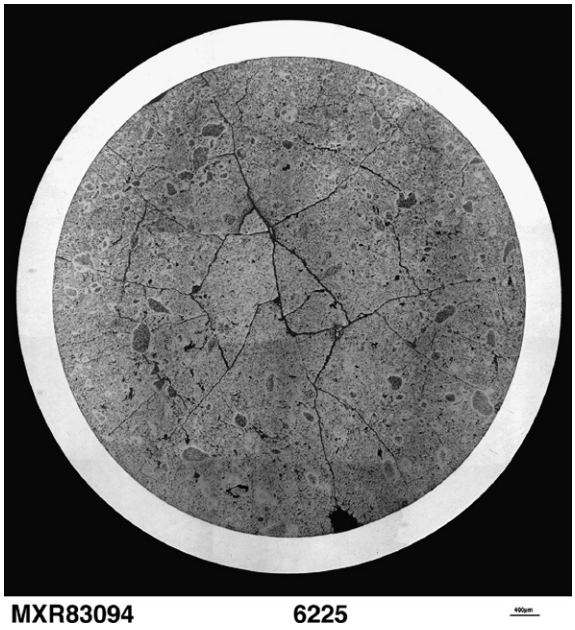

Fig. 4. Cross-section 40 GWd/MT fuel pin. Note the large agglomerates and the halo regions surrounding them. The black region near the bottom is pullout.

the beginnings of the transformation to high-burnup structure – transformation was delayed for the central region agglomerates because local temperatures remained greater than 1000 °C during the early phases of the irradiation.

No evidence of recrystallization ('rim effect') has been found in the fuel matrix around the pellet circumference. Although the rim area experienced low temperature and local burnups higher than the average for the depleted UO_2 matrix, rim area burnup did not reach 60 GWd/MT.

As a further indication of general fuel behavior, an axial mount was prepared to examine the gross condition of the fuel pellet for excessive swelling or other deformations. Fig. 5 shows that at the 50 GWd/MT point fuel behavior was as expected with pellet attributes clearly intact.

7.2. Gallium and fuel swelling

Metallographic and chemical analyses of individual unirradiated test fuel components showed gallium concentrations in the range from 1 to 5 ppm in the fuel (more than 20 times greater than that expected in the mission fuel) and approximately 0.6 ppm in the cladding. If all of the gallium in the fuel were transferred radially outward, the cladding concentration would increase to about 9 ppm. As part of each PIE, samples of irradiated fuel and cladding were sent to the Radioactive Materials Analytical Laboratory at ORNL for determination of the gallium content. The cladding samples have shown insignificant increases in gallium content over the preirradiation gallium concentration. Correspondingly, there has been no evidence of any attack of the inner cladding surface by gallium. Finally, each fuel sample has indicated, within the limits of analytical accuracy, that the gallium initially present has been retained. Post-irradiation fuel and cladding concentration measurements indicate that any movement of this gallium has been insignificant. Initial gallium content in the mission fuel is expected to be two orders of magnitude lower than in the MOX test irradiation fuel.

Comparison of the cladding and pellet dimensions as determined for successively higher burnups establishes the history of pellet swelling and cladding creep as experienced during this test

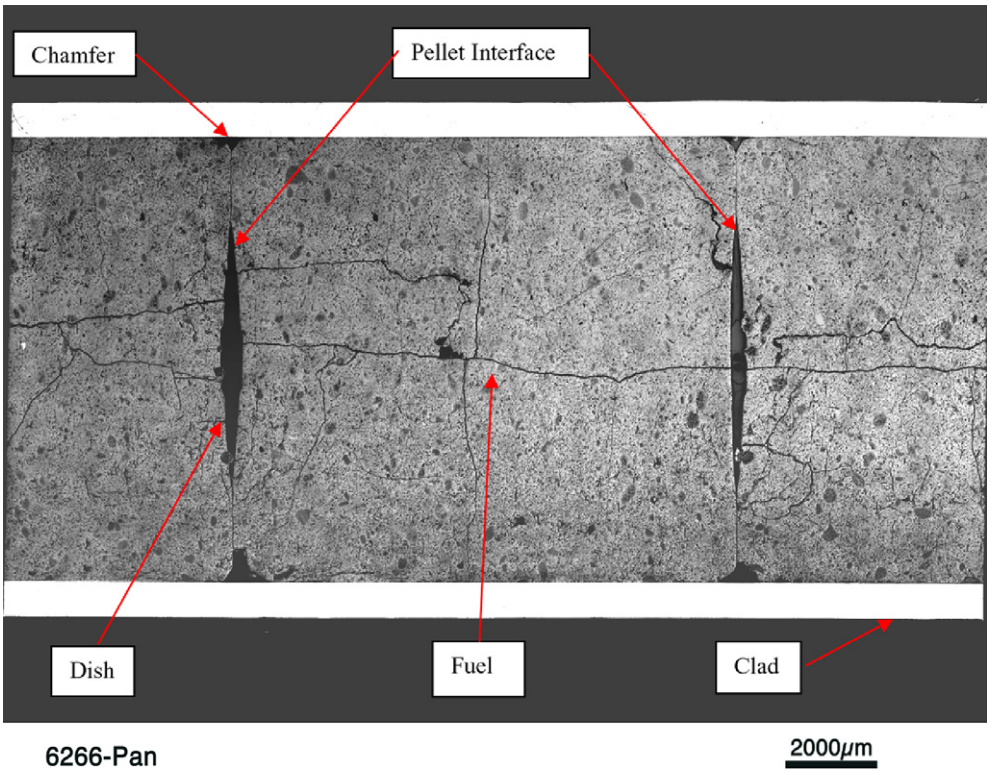

Fig. 5. Transverse Mount at 50 GWd/MT. Note the pellet chamfers and dishing as well as the generally sound conditions of the fuel and cladding. The agglomerates can be clearly seen and the cracking is moderate. There are no signs of excessive swelling.

irradiation. For each of the PIEs completed to date, the capsule and fuel pin metrological results were combined with measurements made directly (imaging software) from photographic enlargements of the metallographic mounts to determine the cladding thickness and internal diameter, the pellet outer diameter, and the effective gap between pellet and cladding. Fuel behavior (cracking, densification, and swelling) is found to be normal and prototypic of commercial MOX fuel [6].

The fuel densification and swelling models within the FRAPCON-3 [7] code accurately reproduce the densification/swelling history for this fuel.

7.3. Cladding outward creep and primary ridging

The fuel pin cladding experienced an irradiation-assisted outward creep under the impetus of a tensile wall (hoop) stress that increased from zero to about 5 MPa as fuel pin internal pressure increased during the irradiation. (This cladding movement differs from normal PWR behavior, where cladding creep down is imposed by high external coolant pressure.) The outward cladding creep (about 0.2%) observed at 40 GWd/MT burnup is normal for the test fuel operating conditions and accumulated fast fluence of $1.4E21$ n/cm^2 ($E > 1.0$ MeV), and is compatible with the experience documented in the literature [8–10]. Fig. 6 shows the measured cladding diameter as a function of length for the 40 GWd/MT case (most aggressive irradiation conditions) as compared to the initial diameter both for the pressurized and unpressurized cases. The final 50 GWd/MT measurement shows similar results.

The fuel pin measuring apparatus developed at ORNL for this project provides a precise determination of the fuel pin outer diameter profile. At all burnup levels, the cladding profiles exhibit local ridging (average radial height about 3.6 μm) over the pellet-to-pellet interfaces. This type of local cladding deformation (denoted 'primary ridging') is commonly observed in commercially irradiated PWR fuel [11,12]. The cause is differential thermal expansion within the fuel – the pellet centerline is much hotter than the outer cylindrical surface and expands axially to a greater extent. The pellets crack into pie-shaped segments, and the differential expansion in the axial direction causes these segments to warp into hourglass shapes.

The formation of ridges in the MOX test fuel pins is somewhat different than in commercial fuel. The high coolant pressure in commercial PWRs causes inward creep of the cladding, which eventually comes into hard contact with the fuel over the pellet interfaces, where the hourglassing produces the largest (deformed) pellet diameters. The cladding primary ridges are therefore artifacts of the hourglass (or saddle) shape of the underlying pellets. The improved heat transfer afforded by cladding creep down (instead of outward cladding

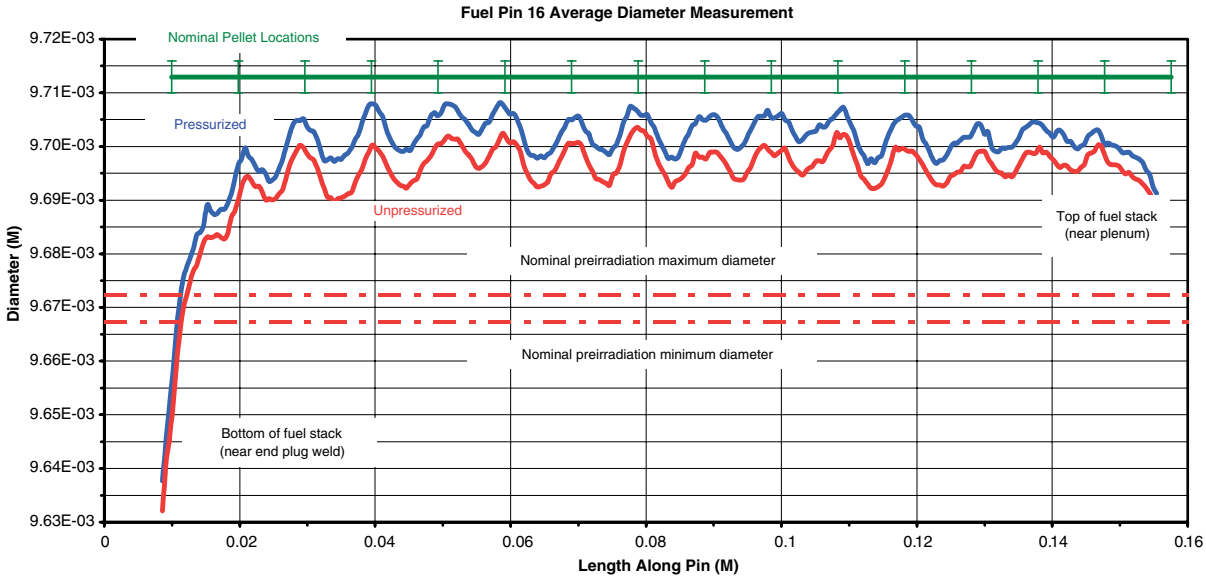

Fig. 6. Fuel pin cladding as a function of length for the 40 GWd/MT exposure. Note the small decrease in diameter for the depressurized case (pin opened for gas measurement) and the general outward creep.

movement) serves to reduce the fuel temperatures at comparable LHGRs.

For the MOX test fuel pins, the pressure differential is outward across the cladding, which creeps outward, not inward. Localized contact between pellet and cladding still occurs, however, because the fuel pins were designed to have initial pellet–clad radial gaps (25 μm) much smaller than found in commercial fuel (75–100 μm). Here the pellet differential thermal expansion is sufficient to cause hourglass-enhanced local contact with the cladding at initial heatup. This hard contact over the pellet-to-pellet interfaces occurs before any fuel densification or swelling.

ABAQUS [13] code finite-element calculations performed for the zero-burnup initial heatup with as-built dimensions for the pellet, fuel pin, and capsule, and with the actual initial LHGRs clearly predict pellet hourglassing with cladding contact at the pellet ends. The applied stress is sufficient to induce local yielding.

To recap, the observed ridging is predicted to have occurred on initial heatup at zero burnup. Primary ridging is expected for modern PWR fuel, and does not constitute a mechanism for failure during normal operation. There is no indication for the current test fuel that such localized contact has had any detrimental effect on cladding integrity.

7.4. Cladding inner surface oxidation

The nature of the corrosion layers intermittently located along the pellet–clad interface is of interest to the examination of cladding performance. These layers exist along the portions of the cladding inner surface where the fuel was in contact with the cladding during irradiation.

The uneven and noncontiguous nature of the corrosion observed on the cladding inner surfaces is an artifact of the manner in which the pellet fragments came into contact with the cladding during irradiation. Inner surface oxidation requires that excess oxygen be available from the fission process and that the fuel be in contact with the cladding to provide a path for solid-state athermal diffusion of the oxygen atoms. The thicker oxidation layers in regions where an agglomerate is located at or near the fuel surface follow directly from the narrower local pellet–clad gaps during irradiation when these agglomerates are swollen. The observed corrosion patterns are in accordance with expectations based on US and European experience with both UO_2 and MOX fuels [14]. Fig. 7 shows an interaction between a surface agglomerate and the cladding (50 GWd/MT). A modest oxide layer of about 15–20 μm forms adjacent to the agglomerate; oxide

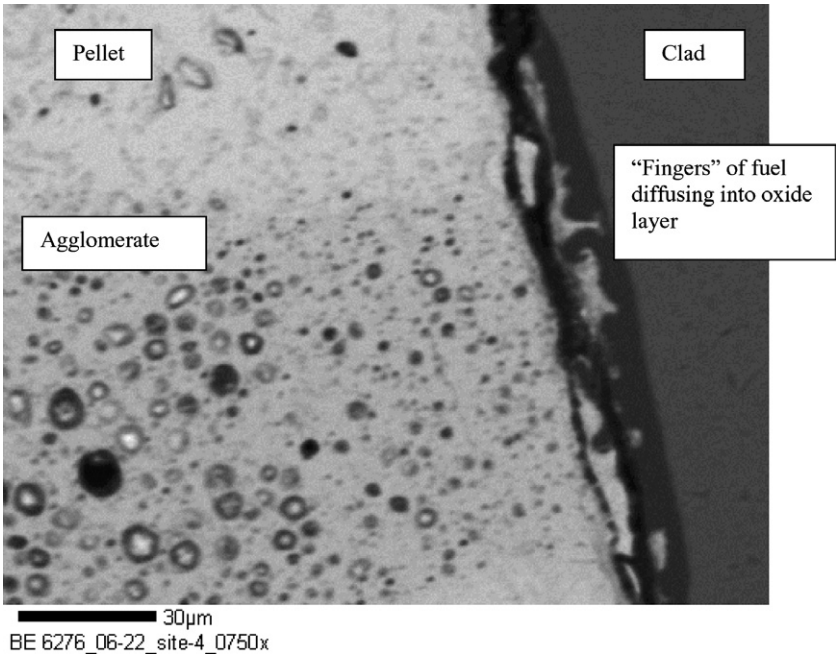

Fig. 7. SEM image of 50 GWd/MT fuel agglomerate/clad region. Oxidation is greatest near an agglomerate; even so, the interaction region is small.

layers away from an agglomerate are much thinner and display no fuel diffusion structure.

7.5. Fission gas release versus MOX experience in Europe

Fig. 8, which is adapted from Ref. [6], illustrates literature values for fission gas release of European commercial test fuels plotted against the corresponding average linear heat generation rates (LHGRs) during the second irradiation cycle.

In general, in the first three irradiation cycles in commercial reactors, the LHGRs increase slightly in proceeding from the first to the second cycle, and in all cases, decrease from the second to the third cycle.

Because the highest powers are experienced during the second irradiation cycle, the average LHGR during that cycle is chosen as the abscissa parameter in Fig. 8. The exception is for cases where the fuel was irradiated just one cycle – here, the fission gas release is plotted against the average LHGR for that single cycle.

Since fuel temperatures are determined by the LHGRs, the points plotted on Fig. 8 can be considered to indicate the linear relation (on a logarithmic scale) between the accumulated gas release at the end of the irradiation and the highest temperature experienced by the fuel during the irradiation. This demonstrates that the fission gas release fraction is determined by the temperature history rather than by the burnup extent. (The *amount* of gas release does, of course, increase in proportion to burnup.)

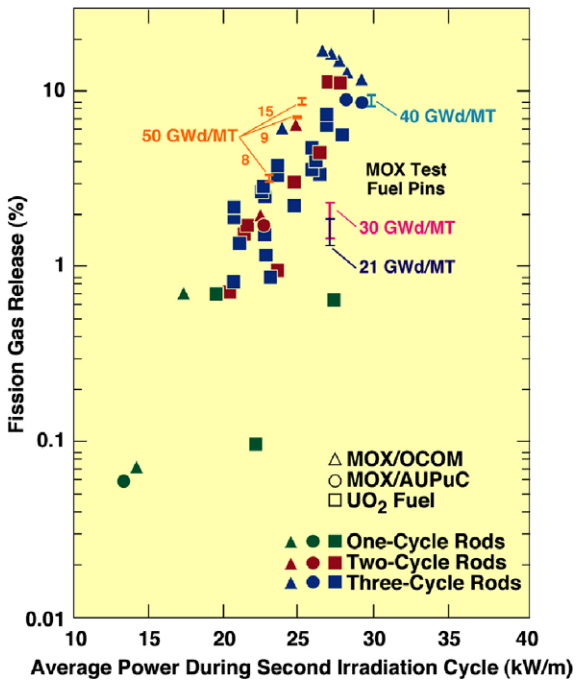

Fig. 8. The MOX test fuel pin gas release fractions can be correlated with their LHGR experience. Basic plot is taken from Ref. [6].

Superimposed on the plot of Fig. 8 are the fission gas release fractions as obtained by Krypton-85 activity measurements for the 21-, 30-, 40-, and 50-GWd/MT burnup fuel pins of the MOX irradiation test. The abscissa values for these release fractions are the average LHGRs during Phase II of the MOX test irradiation.

It is clear from Fig. 8 that the fission gas release fractions obtained for the MOX test irradiation are consistent with the literature values (European experience [6]) for both MOX and UO_2 fuels with the same LHGR history.

7.6. Synopsis of MOX test fuel behavior

The test fuel has been found to perform well, and in accordance with expectations based on the documented European experience. The presence of a few very large agglomerates has not adversely affected fission gas release. No abnormal behavior has been observed. (With respect to the MOX test fuel, 'abnormal behavior' is defined as any deviation from expectations based on the documented MOX fuel irradiation experience in Europe that cannot be explained solely by differences in fuel preparation or test conditions. As an example, the cladding creeps outward in this test as opposed to inward in the commercial MOX experience, but this difference is readily explained by the absence of external coolant pressure on the MOX test fuel pins.)

In addition to demonstrating the applicability of the European database, these PIEs of similar MOX fuels at five burnup intervals offer unique opportunities to study the effects of burnup and irradiation history on MOX fuel performance characteristics.

8. Code predictions

Because of their sequential (and symmetrical) placements in the higher-power locations within the test assembly, Capsules 4 and 13, withdrawn at 40 GWd/MT burnup, experienced the highest LHGRs during this test irradiation. Conversely, Capsule 5, withdrawn at 50 GWd/MT, was most

often located in a low-power region and experienced the lowest LHGRs.

The performance of Capsule 4 (Fuel Pin 7) and Capsule 5 (Fuel Pin 8) has been simulated with FRAPCON-3 (version 1.3, modified at ORNL for MOX usage), FRAPCON-3 (version 2.0, PNL released version applicable for LEU and MOX), and TRANSURANUS [15] (version v1m3j04). The code models for each fuel pin comprise 15 equal length axial segments (one per fuel pellet, with node 1 at the fuel stack bottom and node 15 at the top) and use the axial power peaking factors (as a function of burnup) calculated by use of the MCNP [16,17] code at INL. As stated earlier, the upper and lower ends of the pellet stack are unshielded, the end pellets receive more thermal flux and hence there is end peaking in the fuel stack. Also, the axial peaking is dependent on the capsule position in the test assembly; the effects of both assembly position and end peaking are illustrated in Fig. 9 for Capsule 4 (Fuel Pin 7).

8.1. Capsule 4/Fuel Pin 7 simulations

Since the axial power in the fuel rod is determined via the mean LHGR and the axially-dependent peaking factors, the burnup of each individual pellet is different. The pellet burnup (by Nd-148) ranges for Fuel Pin 7 are illustrated in Fig. 10 and compared with PIE radiochemical analyses [from the Radioactive Material Analysis Laboratory (RMAL) at ORNL]. As indicated, there is excellent agreement between the code predictions (based on the INL MCNP predicted axial peaking factors and cycle LHGRs) and the radiochemical analyses with both the code predictions and the radiochemical analyses illustrating end-peaking in the fuel pellet stack.

The effect of the end peaking on the predicted (FRAPCON-3) fuel centerline temperatures for Fuel Pin 7 is shown in Fig. 11 for nodal positions 1 (bottom pellet), 8 (~centerline of fuel stack), and 15 (top pellet). In Phase II of the irradiation, 155 to 383 days in Fig. 11, the end pellet (nodes 1 and 15) fuel centerline temperatures are 100 to 200 °C higher than at the middle of the fuel stack. However, with depletion of ^{239}Pu in the end pellets, the axial peaking flattens for Fuel Pin 7 (see Fig. 9) and the nodal fuel temperatures converge prior to withdrawal from the reactor (for the period of 700 to 900 days in Fig. 11).

For the majority of Phase II, the predicted fuel temperatures exceed 1300 °C. There is evidence

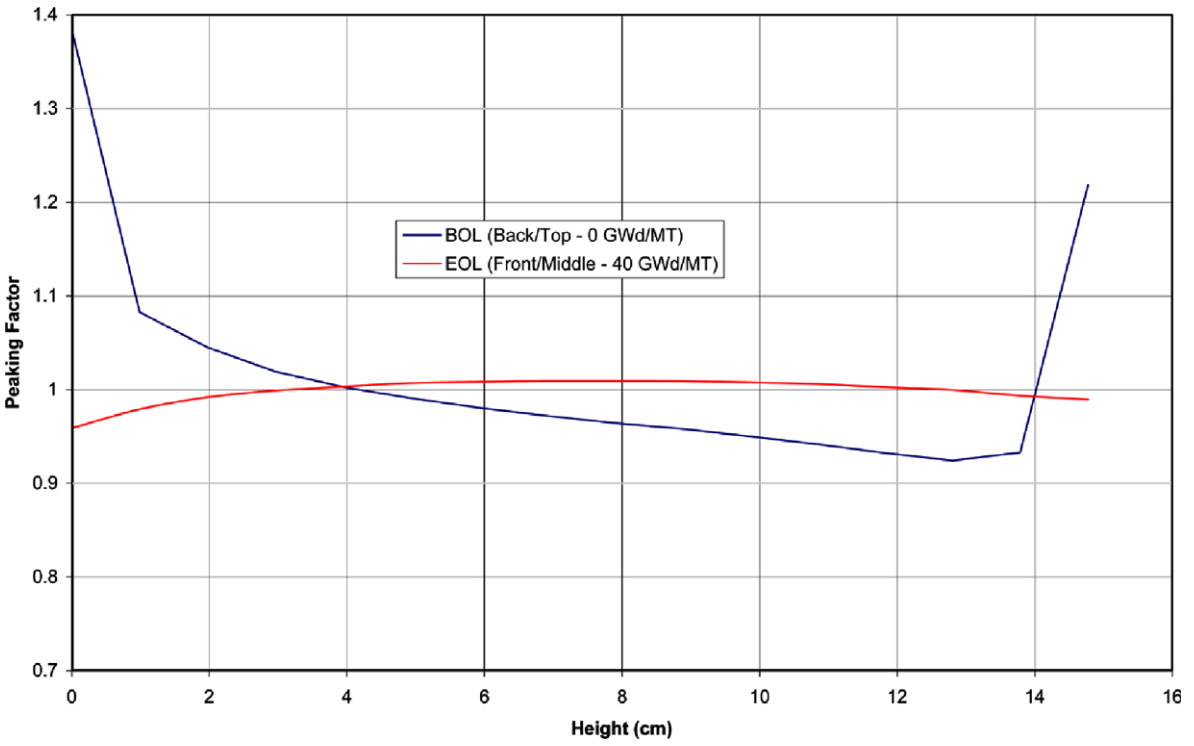

Fig. 9. Capsule 4/Fuel Pin 7 time and position dependent axial power peaking factors.

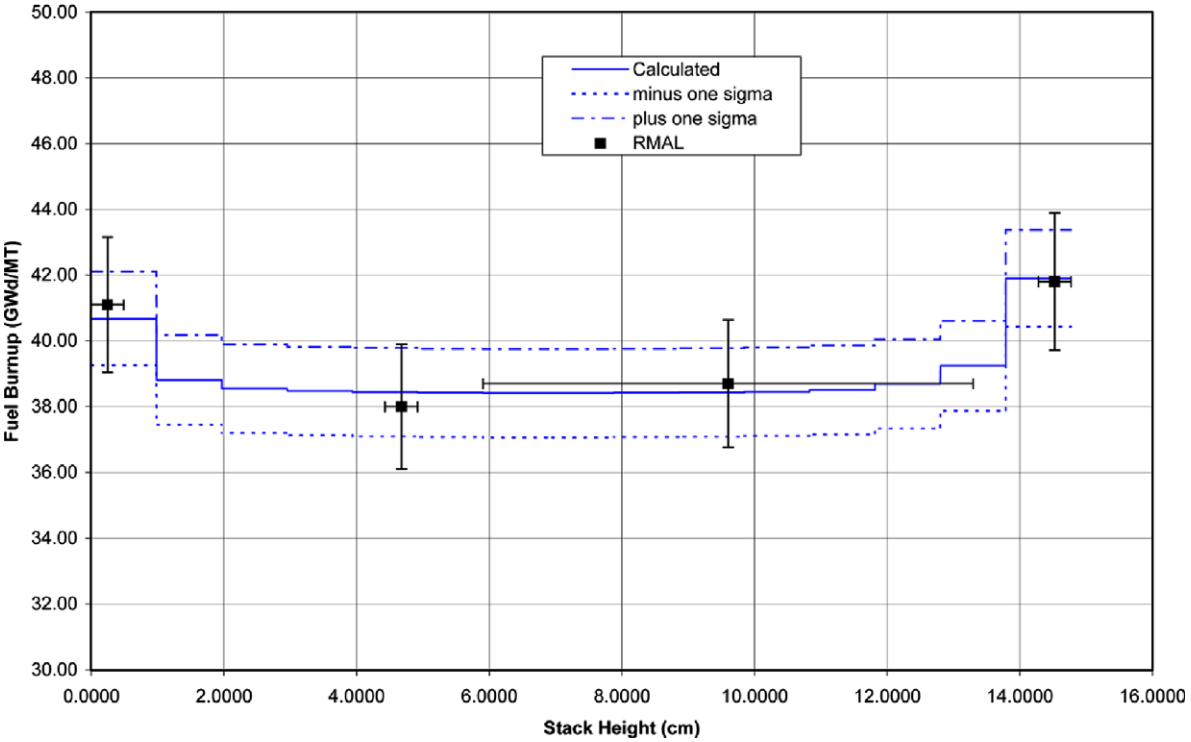

Fig. 10. Capsule 4/Fuel Pin 7 predicted and measured fuel burnup.

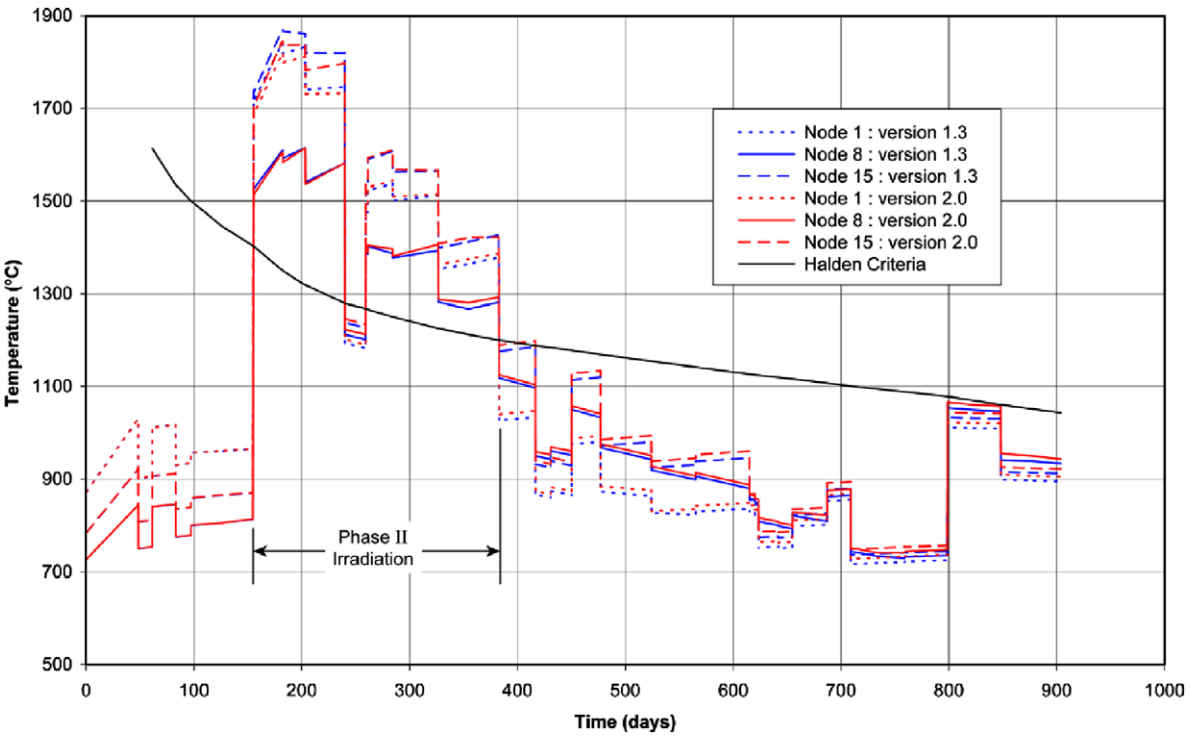

Fig. 11. FRAPCON-3 predicted Capsule 4/Fuel Pin 7 fuel centerline temperatures.

from the PIE capsule gamma scans of ^{137}Cs migration within the fuel stack; this ^{137}Cs migration is in itself evidence that temperatures were in excess of ~1200 °C. On the other hand, the absence of columnar grains in the examined metallographic mounts indicates that these fuel centerline temperatures did not exceed about 1800 °C.

Generally, for irradiation Phase III – Parts 1 and IV – Part 1 (from 383 to 904 reactor-days), the predicted fuel centerline temperatures range from 700 to 1100 °C. From the metallography of Fuel Pin 7, agglomerates are becoming visible toward the centerline of the fuel. The transformation to high-burnup structure that makes these agglomerates readily visible requires local fuel temperatures lower than about 1000 °C.

A comparison of the FRAPCON-3 (versions 1.3 and 2.0) and TRANSURANUS temperature predictions for node 8 is given in Fig. 12. There is good code agreement throughout the simulation for Fuel Pin 7.

Also shown in Fig. 11 are the Halden criteria [18] for fission gas release (greater than 1%). The predicted fuel temperatures exceed the Halden threshold for nearly all of the Phase II irradiation. Thus, a fission gas release for Capsule 4/Fuel Pin 7 of 8.4% (Table 2) is in accordance with the predicted fuel temperatures. Also there is reasonable agreement of the code predictions of the fission gas release (see Fig. 13); at the EOL, the FRAPCON-3 predictions range from 12–13% and TRANSURANUS is closest (~7.1%) to the PIE results.

8.2. Capsule 5/Fuel Pin 8 simulations

As shown in Table 3, Capsule 5 (Fuel Pin 8) has been included in all ATR irradiation phases (approximately 1462 EFPDs), with the lowest LHGRs of all of the irradiated MOX capsules. Except for Phase II when Capsule 5 achieved a LHGR of 23.1 kW/m, Capsule 5's LHGRs have been less than the planned average power for the disposition MOX lead assemblies at BOL (~21 kW/m).

In contrast to the code predictions for Capsule 4, there are significant differences in the temperature predictions for Capsule 5, as shown in Fig. 14. The spread in the temperature predictions at times less than 155 days are due to differences in the code fuel thermal conductivity correlations and, at times greater than 155 days, due to differences in the fission gas release (see Fig. 15) and subsequent decrease of

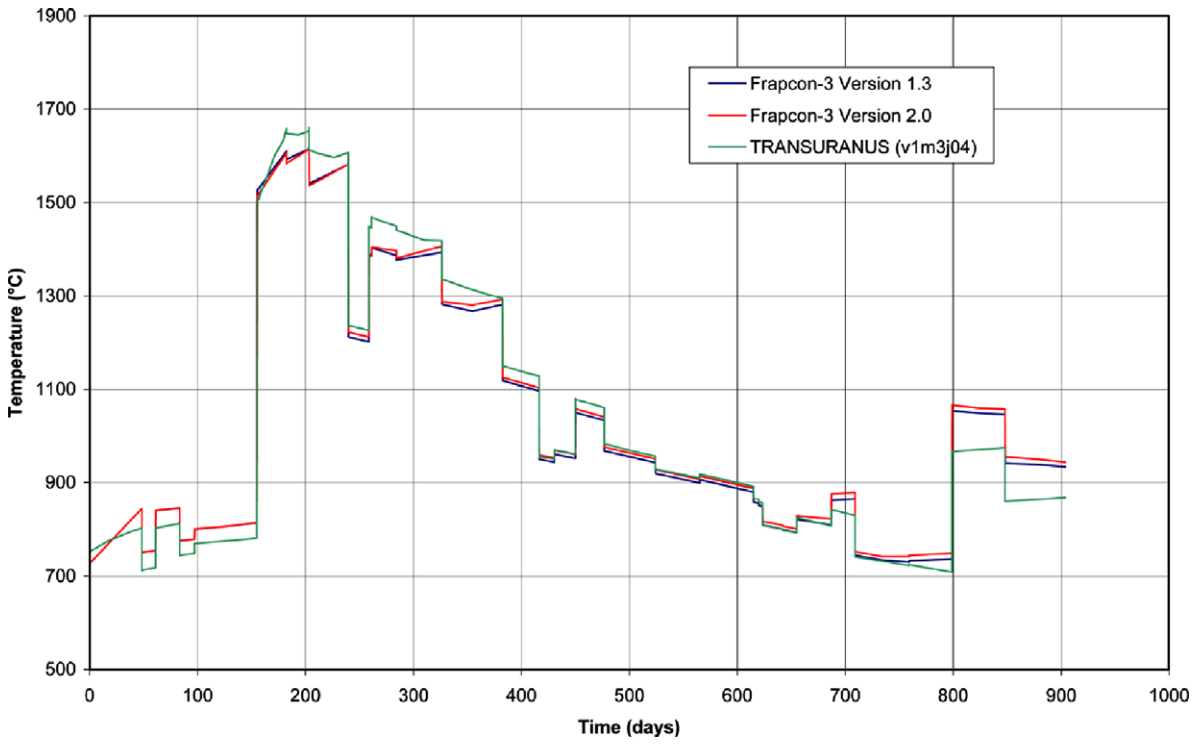

Fig. 12. Code predicted fuel centerline temperatures for Fuel Pin 7 at fuel stack midplane.

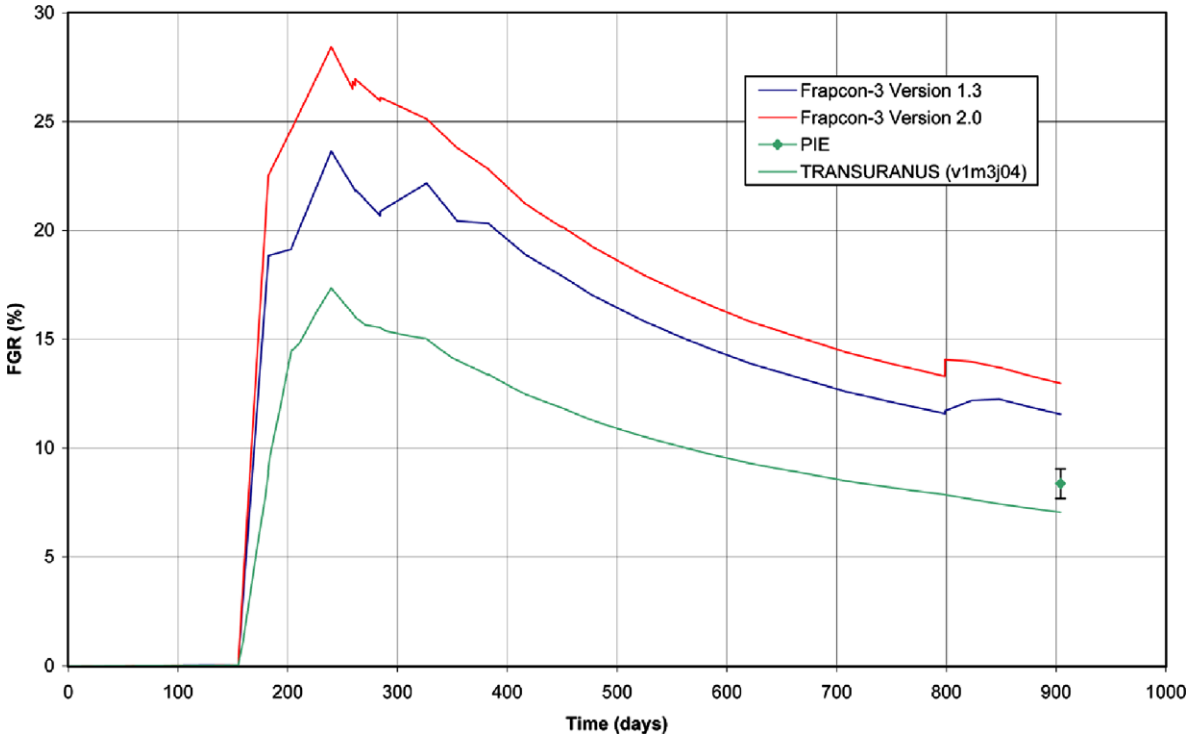

Fig. 13. Predicted and measured fission gas release for Fuel Pin 7.

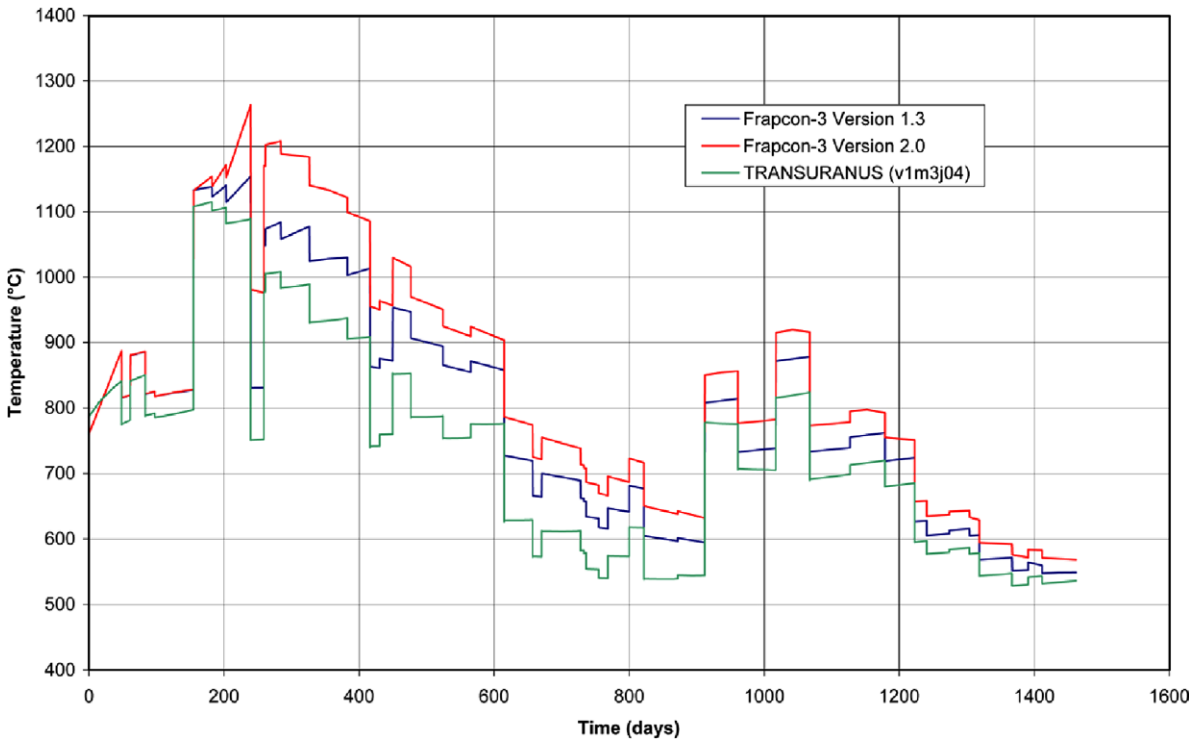

Fig. 14. Code predicted fuel centerline temperatures for Fuel Pin 8 at fuel stack midplane.

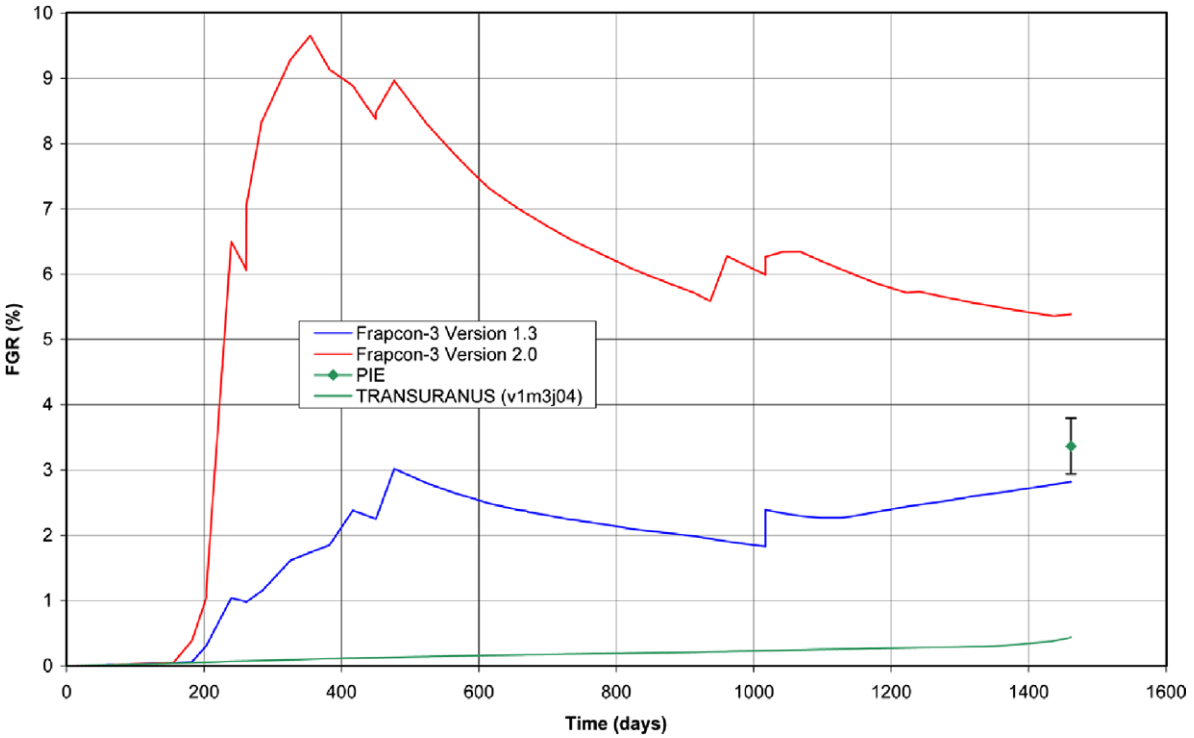

Fig. 15. Predicted and measured fission gas release for Fuel Pin 8.

the gap conductance. During the Phase II irradiation, end pellet temperatures are predicted to approach (maybe exceeding) the Halden criteria for the FRAPCON-3 simulations but not in the TRANSURANUS simulation; thus, the higher predicted fission gas release for the FRAPCON-3 calculations.

Obviously, the low power duties of Capsule 5, during its irradiation, present a modeling challenge for these fuel performance codes which quite accurately predict the performance of the high-duty Capsule 4.

9. Summary

The test MOX fuel prepared with weapons-derived plutonium exhibits normal fuel swelling, densification and fission gas release. The cladding and fuel behavior has been as expected from the literature and is reasonably predicted by available computer codes (i.e., TRANSURANUS and FRAPCON-3).

The MOX irradiation experimental operating envelope (LHGRs and fuel temperatures) is prototypic of commercial light water reactors with fuel of similar dimensions; however, the test fuel has been irradiated under conditions more severe than will be encountered during the fissile material disposition mission. The thermal behaviors of the eleven irradiated MOX capsules are bounded by Capsules 4 and 5.

Fuel performance for these test irradiations has been excellent.

A weapons-derived MOX fuel benchmark problem (based on the irradiation of Capsules 4 and 5) has been proposed to the OECD/NEA TFRPD (expert group on reactor-based plutonium disposition).

Acknowledgements

The submitted manuscript has been authored by a contractor of the US Government under contract No. DE-AC05-00OR22725. Accordingly, the US Government retains a nonexclusive, royalty-free license to publish or reproduce the published form of this contribution, or allow others to do so, for US Government purposes.

Research was sponsored by the Office of Fissile Materials Disposition, US Department of Energy, National Nuclear Security Agency, under Contract DE-AC05-00OR22725 with UT-Battelle, LLC.

References

[1] Department of Energy, National Nuclear Security Administration, Amended Record of Decision for the Surplus Plutonium Disposition Program, 67 FR 76, Office of the Federal Register, Washington, DC, 19 April, 2002.
[2] S.A. Hodge, L.J. Ott, in: Presented at the 2004 International Meeting on LWR Fuel Performance, Orlando, Florida, 19–22 September, 2004.
[3] D.G. Kolman et al., J. Nucl. Mater. 283 (2000) 245.
[4] L.J. Ott, in: Presented at the 2004 International Meeting on LWR Fuel Performance, Orlando, Florida, 19–22 September, 2004.
[5] R.N. Morris et al., in: Presented at the 2004 International Meeting on LWR Fuel Performance, Orlando, Florida, 19–22 September, 2004.
[6] W. Goll et al., Nucl. Technol. 102 (April) (1993) 29.
[7] G.A. Berna et al., FRAPCON-3: A computer code for the calculation of steady-state thermal–mechanical behavior of oxide fuel rods for high burnup, NUREG/CR-6534, December 1997.
[8] M.A. McGrath, in: International Topical Meeting on LWR Fuel Performance, American Nuclear Society, Park City, Utah, 10–13 April, 2000.
[9] A. Soniak et al., in: G.D. Moan, P. Rudling (Eds.), Zirconium in the Nuclear Industry: Thirteenth International Symposium, ASTM STP 1423, ASTM International, 2002, p. 837.
[10] M. Limback, T. Andersson, in: E.R. Bradley, G.P. Sahol (Eds.), Zirconium in the Nuclear Industry: Eleventh International Symposium, ASTM STP 1295, American Society for Testing and Materials, 1996, p. 448.
[11] H. Bailly, D. Menessier, C. Prunier (Eds.), The Nuclear Fuel of Pressurized Water Reactors and Fast Reactors – Design and Behaviour, Lavoisier Publishing Inc., Secaucus, NJ, 1999.
[12] C. Bernaudat, Nucl. Eng. Des. 156 (1995) 373.
[13] ABAQUS/Standard User's Manual Version 5.8, Hibbit, Karlsson and Sorensen, Inc., Pawtucket, Rhode Island, 1998.
[14] C.T. Walker, W. Goll, T. Matsumura, J. Nucl. Mater. 245 (1997) 169.
[15] K. Lassmann, J. Nucl. Mater. 188 (1992) 295.
[16] G.S. Chang, MCNP and ORIGEN2 – Calculated Axial, Radial, and Azimuthal Profiles Versus Burnup in the MOX Test Assembly, ORMOX-GSC-10–00, Idaho National Engineering and Environmental Laboratory (INEEL), March 2000.
[17] J. Briesmeister (Ed.), MCNP – A General Monte Carlo N-Particle Transport Code, Version 4C, LA-13709-M, Los Alamos National Laboratory, 2000.
[18] C. Vitanza, E. Kolstad, U. Graziani, in: ANS Topical Meeting on Light-Water Reactor Fuel Performance, Portland, Oregon, 29 April–3 May 1979.